



## **Numerical Characterization Of The Ultimate Capacity Of An Energy Dissipator Under Cyclic Loading**

**J. Ramírez, Centre Internacional en Mètodes Numèrics a l'Enginyeria, Barcelona, Spain**

**G. Bozzo, SLB Devices, Barcelona, Spain**

**J.M Gonzalez, Universitat Politècnica de Catalunya (UPC), Barcelona, Spain**

**F. Rastellini, Centre Internacional en Mètodes Numerics en Enginyeria, Barcelona, Spain**

**L. Bozzo, Luis Bozzo Estructuras y Proyectos S.L., Barcelona, Spain**

### **Abstract**

This study presents a numerical model of a Buckling Delayed Shear Link (BDSL) seismic protection under cyclic loading up to failure. The model aims to predict the failure mode and location of the dissipator under various loading protocols. The model is supported by experimental tests conducted at the University of Lima, Peru, following standard procedures.

The BDSL system is a shear-based energy dissipator with a connection detail designed to transmit force without axial load, allowing free in-plane rotation. It accommodates in-plane displacements exceeding 60 mm. A Finite Element Method (FEM) model is developed, including boundary conditions and prescribed displacement histories. The BDSL is modeled with hexahedral solid elements, and a penalty-based contact algorithm simulates its interaction between the dissipator and its upper connection.

An elastoplastic material law with optimized hardening parameters is implemented. The model incorporates a ductile fracture criterion based on Equivalent Plastic Strain (EPS) and a Triaxial Failure Diagram (TFD) to predict behavior and failure. The numerical predictions show strong correlation with experimental hysteresis curves and energy dissipation patterns. Mode and location of failures are also validated.

Although further refinements are required to capture failure under diverse cyclic paths, the proposed model provides a reliable numerical tool for evaluating BDSL performance. Future developments target larger displacements and alternative geometries. The proposed approach supports improved design of dissipative systems for enhancing seismic resilience in high-risk regions.

**Keywords:** Buckling Delayed Shear Link, Finite Element Method, Seismic energy dissipation, Cyclic behavior, Numerical modeling.

# 1 Introduction

Since the 1980s, seismic protection technologies have become increasingly important in structural design, offering improved material efficiency, seismic performance, and post-earthquake recovery compared to traditional redundancy-based approaches (Bozzo and Barbat, 1999). These systems act as response control mechanisms to enhance structural resilience.

Supplemental energy dissipation devices are classified into base isolation, passive energy dissipation, and active control systems (Soong and Spencer, 2002). While base isolation is effective for low- to mid-rise buildings by decoupling them from ground motion, its application in tall structures is limited by cost, complexity, and vulnerability to failure.

Recent developments in passive systems—such as viscous, viscoelastic, metallic, and friction dampers—have been reviewed in terms of behavior, modeling, and design methodologies (Symans et al., 2008).

Within this framework, the present study focuses on the advanced numerical modeling of the Buckling Delayed Shear Link (BDSL), a passive seismic protection device (Ramirez et al., 2025). The aim is to develop a calibrated FEM model, validated through cyclic tests, to analyze its behavior up to failure and support the development of a machine learning model for predicting structural responses.

## 2 Buckling Delayed Shear Link (BDSL) System

The Buckling Delayed Shear Link (BDSL), derived from the Shear Link Bozzo (SLB) concept, follows the same principle as the eccentrically braced frame (Popov and Engelhardt, 1987). These devices dissipate seismic energy through plastic deformation under shear and enable the design of stiff, ductile structures with minimal earthquake damage.

Given the efficiency of steel under shear, these devices have been applied in masonry and reinforced concrete buildings. They feature milled zones of reduced thickness—called dissipative windows—where deformation is concentrated. Despite being made of isotropic steel, their geometry and large deformations present challenges for accurate numerical modeling.

The original prototypes for masonry walls were validated through numerical and experimental studies (Hurtado and Bozzo, 2008). Early configurations adopted fully restrained bolted ends. Later investigations introduced a battlement connection with fixed–pinned boundaries, which improved performance and allowed deformations up to 30 mm (Nuzzo et al., 2018). Subsequent refinements increased the deformation capacity to 50 mm, with reported improvements in ductility (Bozzo, 2021).

Figure 2.1 illustrates the BDSL system analyzed in this study, which allows deformations up to 60 mm. Figure 2.1(a) illustrates its installation in walls, 2.1(b) the configuration, and 2.1(c) the physical setup.

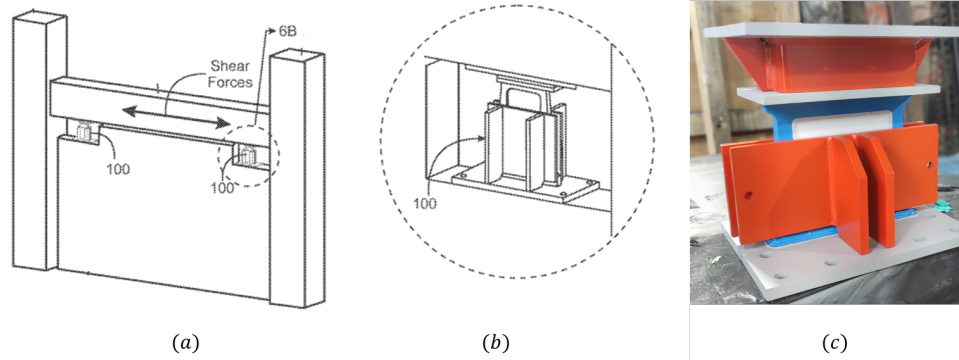


**Figure 2.1 (a) Shear wall test setup with BDSL device; (b) Device location; BDSL device – physical configuration.**

### 3 Experimental Testing

This study used experimental tests conducted at the University of Lima, Peru, employing a  $\pm 1000$  kN hydraulic press to apply shear loads on the cantilevered device. The setup combines simplicity and rigidity to ensure accurate characterization of BDSL dissipators (Bozzo, 2024). This configuration has been used since 2022 for tests reaching up to 80 mm displacement and 700 kN load (Ramirez, 2024). The experimental tests followed ANSI/AISC 341-16 and ASCE 7-22 standards, which define test design, auxiliary element verification, and loading protocols (Figure 3.2a).

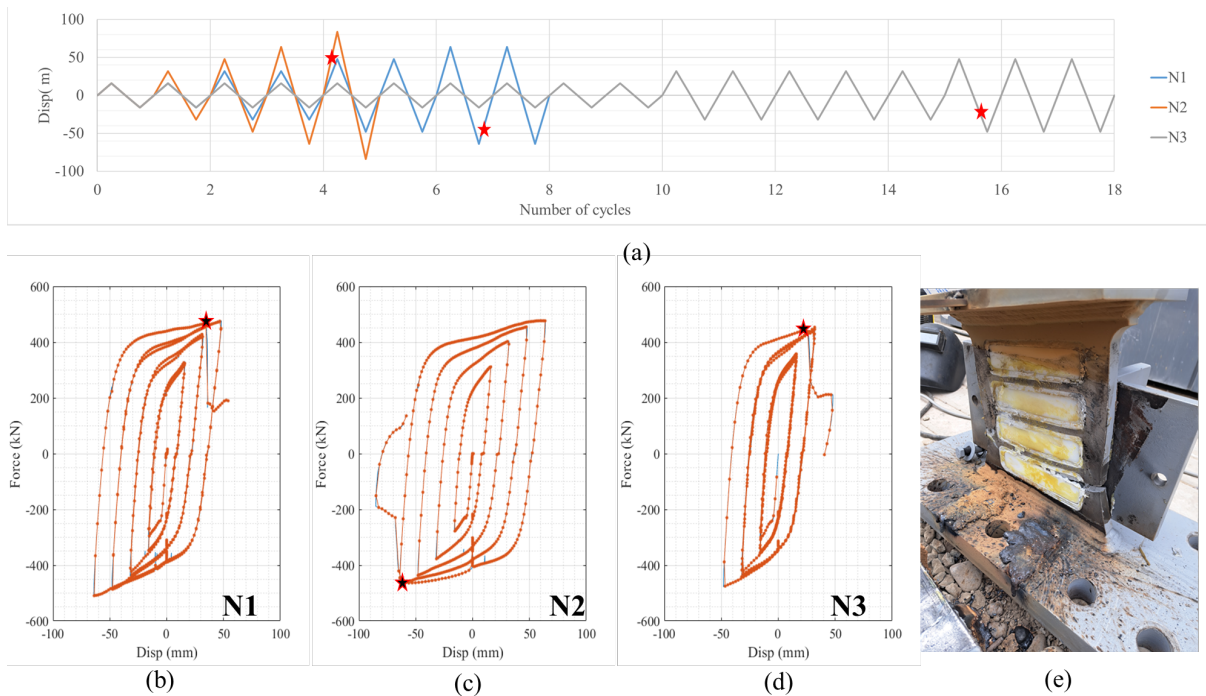


**Figure 3.2. (a) Loading patterns. Hysteretic curves (b-d). (e) N3 failure mode**

The dissipative element consists of a frame with constant thickness and windows of variable geometry. The tested prototype has a total height of 30 mm, a window thickness of 8 mm, and a frame thickness of 25 mm. Three loading patterns were applied to assess the dissipation system, each with varying cycle counts and amplitudes of 16, 32, 48, 64, and 80 mm. Failure points are marked for each test. The hysteresis curves of the devices show distinct failure locations (Figures 3.2b–d), while Figure 3.2(e) illustrates the failure mode from test N3. The failure of the dissipative frame depends on both the amplitude and the number of deformation cycles

## 4 Numerical Modeling of the BDSL System

This section introduces the finite element model used to simulate the BDSL system. It outlines the modeling assumptions, including geometry, material properties, boundary conditions, and contact definition. Calibration procedures are also detailed to ensure accurate response under cyclic loading, forming the basis for comparison with experimental results.

### 4.1 FEM Model of the BDSL System

The numerical models were developed using COMPACK<sup>1</sup>, an explicit dynamic FEM code created at CIMNE for simulating composite structures. The physical configuration of the BDSL system is shown in Figure 4.1a, while the corresponding numerical model appears in Figure 4.1b.

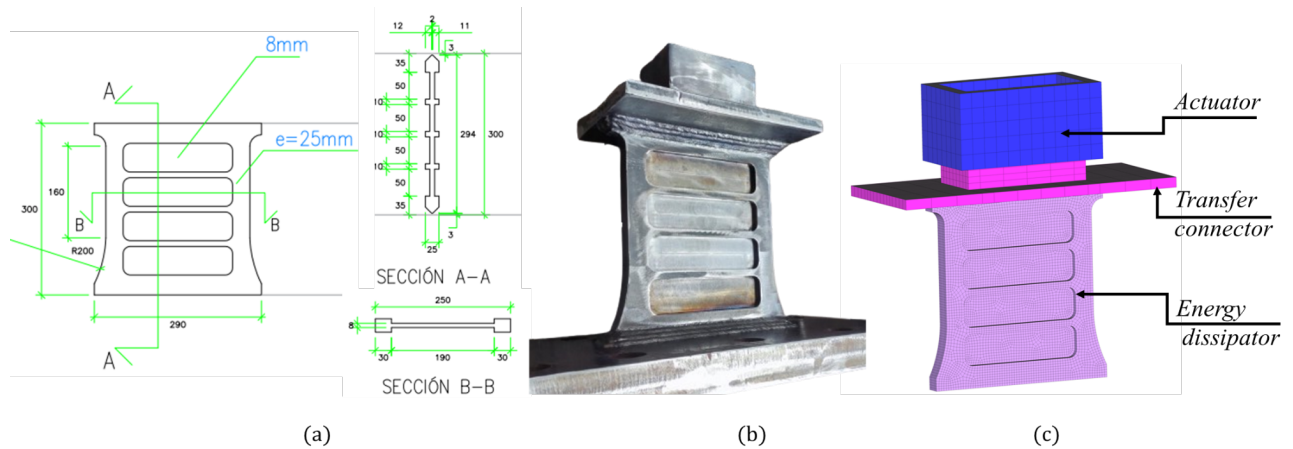


**Figure 4.1. (a) Geometry of the BDSL system. (b) FEM Model of the BDSL system.**

The energy dissipator features a symmetric, variable geometry with rounded-edge windows machined to a reduced thickness to enhance cyclic performance. The rigid frame is defined by specific design parameters. Boundary conditions include a top connection made of rigid parts separated by a 0.5 mm gap to prevent axial force transmission.

The mesh consists of linear 8-node hexahedral solid elements with structured discretization. Gauss point integration ensures accurate shear and volumetric response. Geometric nonlinearities are addressed using a Total Lagrangian formulation with additive decomposition of the logarithmic strain tensor, suitable for capturing large inelastic deformations (Flores, 2001). The

<sup>1</sup> CIMNE, COMPACK: <http://tts.cimne.com/compact/>



representative model, for a given geometry, features a mesh density of 1,076 nodes within the windows and 2,756 nodes in the frame.

## 4.2 Nonlinear Material Behavior of BDSL System

The dissipative components are made of ASTM A36 steel, whose cyclic behavior is modeled using a combined isotropic–kinematic hardening law calibrated for seismic response. Advanced plasticity models, such as the Yoshida-Uemori (Y-U) model, offer improved accuracy in representing phenomena like the Bauschinger effect, softening, and hardening stagnation under large elasto-plastic deformations (Yoshida and Uemori, 2002).

The present research employs the Y–U model, which proves effective for seismic applications by outperforming traditional constitutive laws in simulating both cyclic and monotonic loading. Calibration was performed using parameters proposed in a previous study (Jia and Kuwamura, 2014), as shown in Table 4.1. The material properties used are  $\rho = 7800 \text{ kg/m}^3$ ,  $E = 200 \text{ GPa}$ , and  $\nu = 0.30$ .

**Table 4.1 Material parameters in the Y-U model\***

Plasticity parameters							Parameters for prestrain-dependent Young's moduli		
Y	b	C	m	B	Rsat	h	Eo	Ea	$\xi$
255.9	194.9	338.7	7.9	277.3	196.0	0.50	200	152	30.8

\*Y, b, B, Rsat in MPa; Eo and Ea in GPa

The Triaxiality Failure Diagram (TFD) is a three-dimensional failure criterion with defined safety zones, developed using the COMPACK solver (Rastellini et al., 2016). It relates equivalent plastic strain at failure to stress triaxiality, providing a stress-based framework suitable for predicting material failure. In this study, the triaxial failure curve for ASTM A36 steel was defined using plastic strain and triaxiality values derived from previous studies (Zhuang, 2021).

## 4.3 Boundary and Kinematic Conditions

The contact interfaces in the BDSL system are defined at the actuator and transfer connector, which are modeled as rigid bodies. Contact occurs at two main surfaces, which control interaction between the connection components and the dissipator. These interfaces are defined to prevent axial force transmission while allowing sliding, a key feature in the energy dissipation mechanism. Contact forces at these interfaces are extracted from the FEM model to assess the system's response.

In addition to material nonlinearity, contact interaction represents a key source of nonlinearity in the BDSL system. COMPACK applies a three-dimensional penalty-based algorithm to model this behavior (Zhong, 1993). This study neglects frictional effects.

The FEM model incorporates customized boundary and kinematic conditions to replicate the experimental setup accurately. Figure 4.2a illustrates the main mechanical components of the BDSL system. The setup includes flexible elements connected to the actuator, a transfer connector, a frame, four windows, and a flexible base that replicates realistic boundary conditions.

Displacement measurements obtained from auxiliary tools showed variations linked to the testing machine. To account for this effect, a flexible base was incorporated into the numerical model, adding deformability to the system and improving agreement with experimental results. Although a rigid base was initially considered, elastic hexahedral elements were later introduced beneath the dissipator to represent the system's flexibility better. This modification improved the global response and reduced the initial stiffness observed in the hysteresis curve.

As shown in Figure 4.2b, a prescribed displacement is applied at the top to simulate the actuator, transmitting the load through the connection to the BDSL device. Deformation is concentrated in the steel frame with windows, while a fixed base constrains all displacements. Master-slave conditions are imposed to ensure proper interaction between the transfer connector and the BDSL energy dissipator.

Figure 4.2c illustrates the buckling control planes integrated into the system. Rigid planes are added to prevent out-of-plane deformation of the energy dissipator frame. Additionally, two extra control planes are introduced to restrain local buckling within the four dissipative windows. Two pairs of contact interfaces are defined to guide the deformation through interaction with these rigid planes. This configuration directs the inelastic deformation toward target zones, enhancing control under cyclic loading

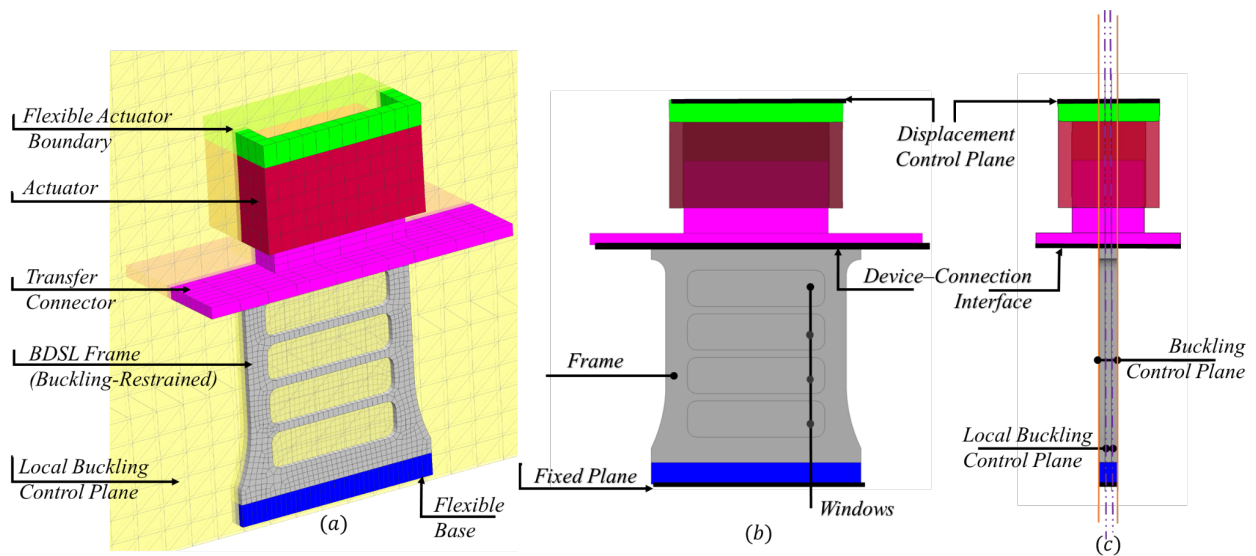


**Figure 4.2. (a) Mechanical configuration of the BDSL system. (b) Boundary and Kinematic Conditions; (c) Global and Local Buckling Control Planes**

## 5 NUMERICAL RESULTS

### 5.1 EXPERIMENTAL – NUMERICAL VALIDATION

This section presents the experimental–numerical correlation. Figure 5.1 compares the hysteretic curves of specimens N1, N2, and N3 from tests and FEM simulations, showing good agreement. Differences in loading and unloading paths, especially in cycles with larger peak displacements, highlight the effect of the applied protocols and show the accuracy of the model calibration over a wide range of loading patterns.

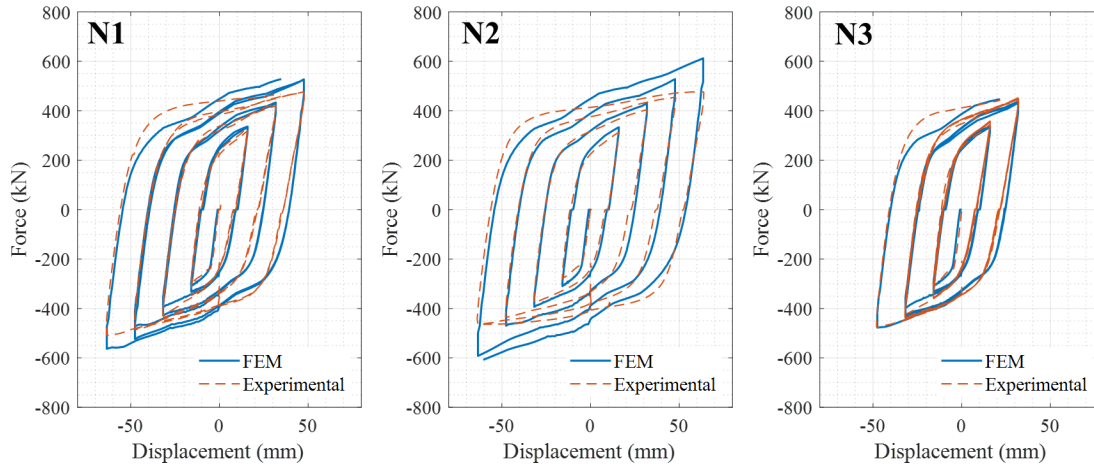


**Figure 5.1. FEM calibration through hysteretic response comparison**

The energy absorbed by the BDSL system corresponds to the area within the hysteresis loops. Figure 5.2 shows the cumulative dissipated energy versus cumulative displacement for tests N1–N3, comparing experimental and FEM results. A close match is observed, though specimens N1 and N2 show slight differences in energy accumulation trends. As expected, energy per cycle increases with displacement, leading to a continuous rise in cumulative energy.

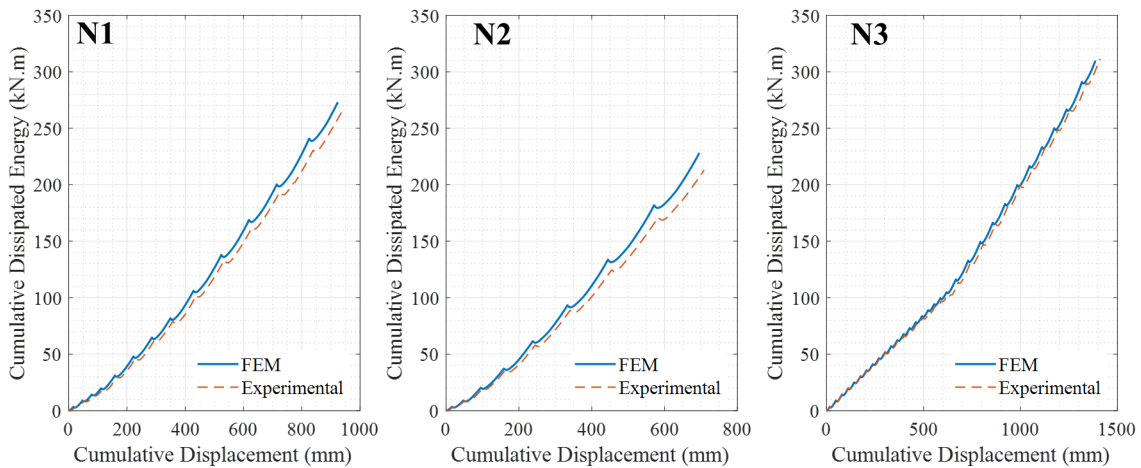
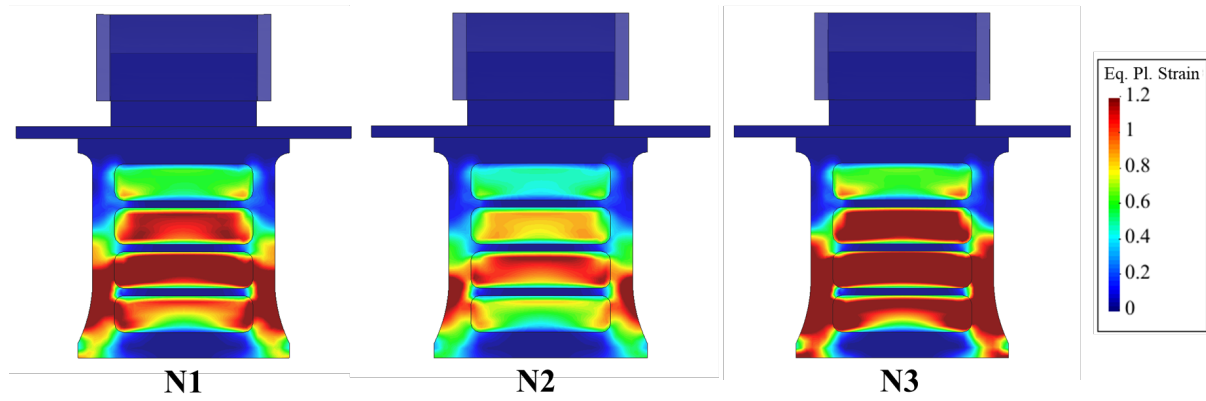


**Figure 5.2. Comparison of cumulative energy dissipation between FEM and experiments**

## 5.2 NUMERICAL RESULTS AND ANALYSIS

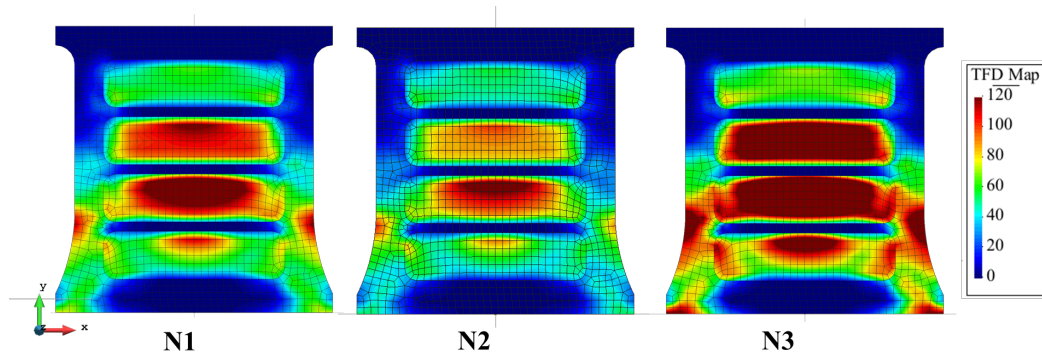
This section presents key results obtained from the FEM simulations under cyclic loading and unloading of the BDSL system. The analysis includes the distribution of equivalent plastic strain, a TFD map, and the estimation of failure. Post-processing of the numerical simulations performed with COMPACK was carried out using the GiD postprocessor. The simulation results were aligned with the failure point recorded during the experiments.

Figure 5.3 presents the EPS distribution for the three cases. The highest plastic strain appears around the windows and in the lower corners of the frame (approximately one-third of the height,  $H \approx 300$  mm), confirming shear-dominated behavior in the windows and axial action in the frame. In N3, strain becomes more widespread and intense. As the frame degrades, the response destabilizes, distorting the hysteresis and indicating structural damage.



**Figure 5.3. Distribution of Equivalent Plastic Strain**

On the other hand, Figure 5.4 shows the Triaxial Failure Diagram (TFD) Map for specimens N1, N2, and N3. The defined failure curve (section 4.2) indicates proximity to material failure under cyclic loading. TFD values increase with higher cycle counts and displacement amplitudes, especially in N3, where large areas approach the critical threshold.



**Figure 5.4. TFD Map of the BDSL Dissipative Element**

To support the previous findings, an analysis was performed on the equivalent plastic strain and triaxiality across all nodes of the FEM model. Figure 5.5 shows the relationship between triaxiality and plastic strain for the frame and window regions, along with the reference failure

curve (TFC). The window zones (orange) concentrate most of the plastic demand, with many points near or above the TFC, especially in specimen N3. These zones show triaxiality values close to 0, indicating shear-dominated behavior. In contrast, the frame zones (blue) show a wider but lower strain distribution, with higher triaxiality values around  $1/3$ , which are typical of axial tension. Compression is not considered critical here, as cracks tend to close. However, the higher global strain levels in the frame suggest that its failure could compromise the entire system, as confirmed by the test. As loading progresses, more nodes reach critical conditions, reinforcing the energy-dissipating role of the windows and the increasing risk of failure.

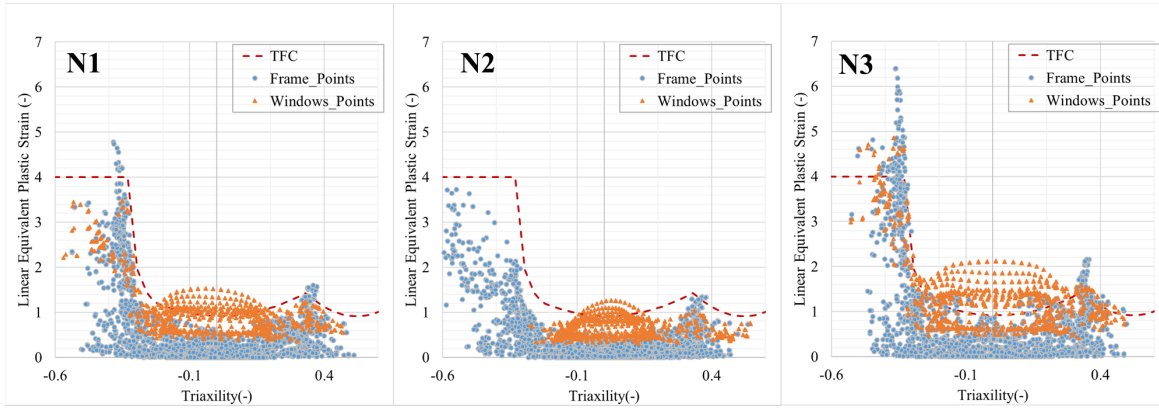


**Figure 5.5. Triaxiality vs. Equivalent Plastic Strain compared to the TFC**

Finally, Figure 5.6 presents the TFD-based safety zone map for specimen N3, highlighting varying levels of structural demand. This analysis confirms the value of the TFD criterion in identifying critical regions under seismic loading, with zones ranging from compression to failure.

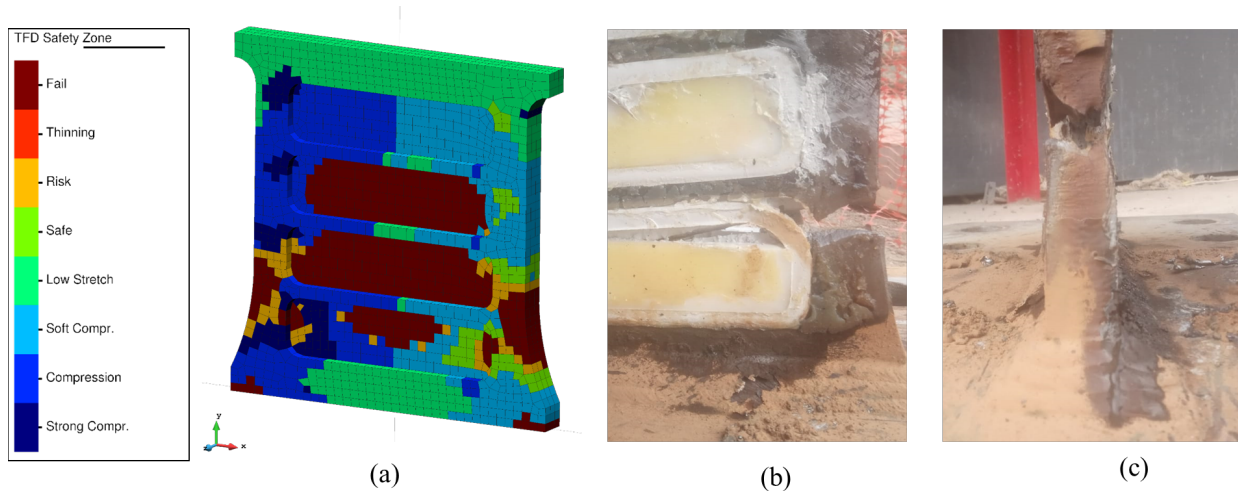


**Figure 5.6. FEM and experimental failure mode for N3**

The results reveal concentrated damage in the window areas, where several regions reach risk or failure thresholds. The large number of low-amplitude cycles suggests potential failure due to ultra-low-cycle fatigue. Figure 5.6(a) shows the FEM-based safety map, while Figure 5.6(b) displays the damaged specimen after testing, with evident deformation. Figure 5.6(c) offers a

close-up of the failure area, where the frame experienced severe damage. The comparison between the simulation and the experiment shows strong agreement, reinforcing the reliability of the FEM predictions and matching the damaged region observed in the corresponding experiment.

## 6 CONCLUSIONS

This study presents a numerical model of the BDSL system under cyclic loading, supporting the development of a numerical-experimental methodology to characterize the structural response. A finite element model incorporates appropriate boundary conditions, contact interactions among components, a constitutive law, nonlinear formulations, and a failure criterion to predict structural response.

After calibrating the constitutive parameters, the numerical results showed good agreement with the experimental data in key performance indicators, including hysteresis curves and energy dissipation.

The calibration process achieved close correspondence with laboratory observations, confirming the model's ability to reproduce the behavior of the physical device. In addition, the model accurately captures the failure mode and its location in each component of the system—both frame and window—taking into account their respective triaxiality conditions.

## 7 ACKNOWLEDGEMENTS

The authors acknowledge the financial support of Projecte ACE100/23/000022 – *Edificacions resilientes equipades amb dissipadores Shear Link*, funded by the Government of Catalonia through ACCIÓ, with support from the Catalan Office for Climate Change, and in collaboration with *Luis Bozzo Estructuras y Proyectos S.L.* and the *Centre Internacional en Mètodes Numèrics a l'Enginyeria* (CIMNE).

## References

- ANSI/AISC 341-16 (2016). Seismic Provisions for Structural Steel Buildings. American Institute of Steel Construction, Chicago.
- ASCE (2021). ASCE/SEI 7-22 Standard: Minimum Design Loads and Associated Criteria for Buildings and Other Structures. American Society of Civil Engineers, Reston, VA.
- Bozzo, G. (2021). *Una nueva generación de disipadores SLB “Shear Link” para el diseño sismorresistente*. Master’s thesis, Universitat Politècnica de Catalunya, Barcelona.
- Bozzo, L.M. & Barbat, A.H. (1999). Diseño sismorresistente de edificios – Técnicas convencionales y avanzadas. Reverté, Barcelona.
- Bozzo, L.M., Ramirez, J., Bairan, J., Bozzo, G. & Muñoz, E. (2020). Precast buildings equipped with SLB seismic devices. In Proc. 17th World Conference on Earthquake Engineering.



- Flores, F.G. (2001). Elementos finitos para el análisis de sólidos anisótropos con grandes deformaciones plásticas. *Mecánica Computacional*, 5, 171–178.
- Hurtado F., Bozzo L. (2008) Numerical and experimental analysis of a shear-link energy dissipator for seismic protection of buildings. In *Proc. 14th World Conference on Earthquake Engineering*.
- Jia, L.-J. & Kuwamura, H. (2014). Prediction of cyclic behaviors of mild steel at large plastic strain using coupon test results. *Journal of Structural Engineering*, 140(2), 04013056.
- Martinez, X., Oller, S., Rastellini, F. & Barbat, A. (2008). A numerical procedure simulating RC structures reinforced with FRP using the serial/parallel mixing theory. *Computers & Structures*, 86(15–16), 1604–1618.
- Nuzzo, I., Losanno, D., Caterino, N., Serino, G. & Bozzo Rotondo, L.M. (2018). Experimental and analytical characterization of steel shear links for seismic energy dissipation. *Engineering Structures*, 172, 405–418.
- Popov, E.P., Kasai, K. & Engelhardt, M. (1987). Advances in design of eccentrically braced frames. *Bulletin of the New Zealand National Society for Earthquake Engineering*.
- Ramírez M., J.; Bozzo, G.; Gonzalez, J.M.; Rastellini, F.G.; Irazábal, J.; Bozzo, L. (2025). Advanced Modeling of Buckling Delayed Shear Links under Strong Cyclic Loads. *COMPDYN 2025: Computational Methods in Structural Dynamics and Earthquake Engineering – Proceedings of the 10th International Conference on Computational Methods in Structural Dynamics and Earthquake Engineering*, streamed from Athens, Greece, 15–18 June 2025. Institute of Structural Analysis and Antiseismic Research, 2025. [Format for conference proceedings]
- Rastellini, F., Socorro, G., Forgas, A. & Oñate, E. (2016). A triaxial failure diagram to predict the forming limit of 3D sheet metal parts subjected to multiaxial stresses. *Journal of Physics: Conference Series*, 734(3), 032020.
- Soong, T.T. & Spencer, B.F. (2002). Supplemental energy dissipation: state-of-the-art and state-of-the-practice. *Engineering Structures*, 24(3), 243–259. DOI: 10.1016/S0141-0296(01)00092-X. [explore.openalex.org](https://www.explore.openalex.org)
- Symans, A., Charney, C., Whittaker, D., Constantinou, M., Kircher, C., Johnson, M. & McNamara, R.J. (2008). Energy Dissipation Systems for Seismic Applications: Current Practice and Recent Developments. *ASCE Journal of Structural Engineering*, 134(1), 3–21. DOI: 10.1061/(ASCE)0733-9445(2008)134:1(3).
- Yoshida, F. & Uemori, T. (2002). A model of large-strain cyclic plasticity describing the Bauschinger effect and work-hardening stagnation. *International Journal of Plasticity*, 18(5–6), 661–686.
- Zhong, Z. (1993). *Finite Element Procedures for Contact Impact Problems*. Oxford Univ. Press, Oxford.
- Zhuang, C. et al. (2021). Ductile fracture characterization of A36 steel and comparative study of phenomenological models. *Journal of Materials in Civil Engineering*, 33(1), 04020421.